JOURNAL OF THERMOPHYSICS AND HEAT TRANSFER
Vol. 13, No. 4, October-December 1999

Heat Transfer in Natural Convection of Magnetic Fluids

H. Yamaguchi,* I. Kobori,† and Y. Uehata‡
Doshisha University, Kyoto 610-0321, Japan

The natural convection of a magnetic fluid in a two-dimensional rectangular cavity with an imposition of an even vertical magnetic field was studied experimentally and numerically. Results obtained from the numerical analysis showed good agreement with experimental heat transfer data. From both experiment and numerical analysis, it was revealed that the vertically imposed magnetic field has a destabilizing influence, and at the super critical state the flow mode becomes substantially different from that with no magnetic field. A prediction from the numerical analysis indicates that the imposition of the magnetic field causes the flow to a higher transition flow mode, enhancing the heat transfer.

Nomenclature

AR = aspect ratio
$\boldsymbol{B}$ = magnetic induction vector
Br = Brinkmann number
C = specific heat
g = gravitational acceleration
H = strength of magnetic field
$\boldsymbol{H}$ = magnetic field vector
H_0 = strength of external magnetic field
K = pyromagnetic coefficient
$\boldsymbol{M}$ = magnetization vector
M_s = saturation magnetization
Pr = Prandtl number
p = pressure
Ra = Rayleigh number
Ra_c = critical Rayleigh number
Ra_m = magnetic Rayleigh number
T = temperature in the cavity
T_s = Curie temperature
T_0 = reference temperature
t = time
$\boldsymbol{v}$ = velocity vector
y, z = coordinate system
α = volumetric expansion ratio
ζ = vorticity
η = viscosity
κ = thermal diffusivity
λ = thermal conductivity
μ_0 = permeability in vacuum
ρ_0 = reference density
ϕ = stream function
χ = susceptibility
ψ = magnetic field potential

I. Introduction

MAGNETIC fluid, which posses both magnetic and flow properties, has many applications in the thermofluid engineering field.[1] Magnetic fluid heat transfer characteristics research and the flow behavior of natural convection are of interest in science and engineering where an imposition of a magnetic field influences hydrodynamic states.[2–5] The natural convection of a magnetic fluid is attractive in space engineering, where the gravity acceleration can be replaced by a magnetic body force. Furthemore, thermomagnetic free convection in a magnetic fluid is known to be significantly greater than ordinary natural convection (Benard convection),[2,6] increasing the efficiency of cooling devices such as electric transformers. Blennerhassett et al.[4] examined heat transfer characteristics and the hydrodynamic instability of a magnetic fluid for an infinite slab by using weakly nonlinear analysis and calculated the Nusselt number in the vicinity of the first critical state, indicating the destabilizing influence of the magnetic field and an increase of the heat transfer rate (15%). The spatial variation in magnetization (considering the magnetic field perturbation) is well presented by Finlayson[7] for the natural convection of magnetic fluids when the magnetization (which depends on the temperature and temperature gradient) is established across the flat infinite slab. Thus far, attempts to study the natural convection of a magnetic fluid have been limited only to the infinite slab,[2–4] although in many actual cases the rigid side walls that make up a confined enclosure are inevitable.[5] More recently, Yamaguchi et al.[8] showed experimentally the flow modes and heat transfer characteristics for a square cavity when a vertical magnetic field was imposed, with the aid of a numerical simulation. Although some primary results for the square cavity case were obtained and arguments were made against the destabilizing effects of the magnetic field,[8] neither the detailed flow transition nor its associated heat transfer characteristics were investigated for the various geometries of the confined enclosure with different aspect ratios, that is, the ratio of the vertical and horizontal length in a two-dimensional cavity.

In the present study the natural convection of a magnetic fluid in a bottom-heated square cavity with two insulated rigid side walls (which form a two-dimensional rectangular cell) is studied experimentally and analytically for the externally imposed magnetic field. An experiment is conducted to obtain the heat transfer characteristics when a temperature-sensitive magnetic fluid, filled in the cavity whose aspect ratios are 1.0, 1.5, and 2.0 (with 0.5 depth ratio assuming the two dimensionality), is heated from the lower wall and cooled at the upper wall. The vertical uniform magnetic field is imposed to the cavity externally, and heat transfer characteristics are obtained from temperature measurement. A numerical analysis based on the finite difference method is also carried out to verify the experimental results and to investigate a relevant flowfield associated with the experimental data.

II. Experimental Arrangement

The magnetic fluid used in the experiment is the temperature-sensitive magnetic fluid, Mn–Zn ferrite in an alkyl-naphthalene base, whose magnetization $\boldsymbol{M}$ for the temperature T and magnetic field $\boldsymbol{H}$ can be approximated, assuming a linear magnetization[7] relation, as follows:

$$\boldsymbol{M} = [\chi - K(T - T_0)]\boldsymbol{H} \tag{1}$$

Received 3 February 1999; revision received 4 June 1999; accepted for publication 23 June 1999.

*Professor, Department of Mechanical Engineering; hyamaguc@mail.doshisha.ac.jp.
†Professor, Department of Mechanical Engineering; imtj-Ko@qa2.so-net.ne.jp.
‡Postgraduate Student, Department of Mechanical Engineering.

Table 1 Properties of magnetic fluid

Parameter	Value
Density ρ_0, kg/m^3	1.279×10^3
Viscosity η, Pa · s	3.826×10^{-1}
Thermal conductivity λ, W/(m · K)	6.917×10^{-1}
Thermal diffusivity κ, m^2/s	1.656×10^{-7}
Coefficient of cubical expansion α, 1/K	4.587×10^{-3}
Saturation magnetization M_s, G	3.40×10^2
Curie temperature T_s, K	477.32
Reference temperature T_0, K	298.15
Susceptibility χ	2.675×10^{-1}

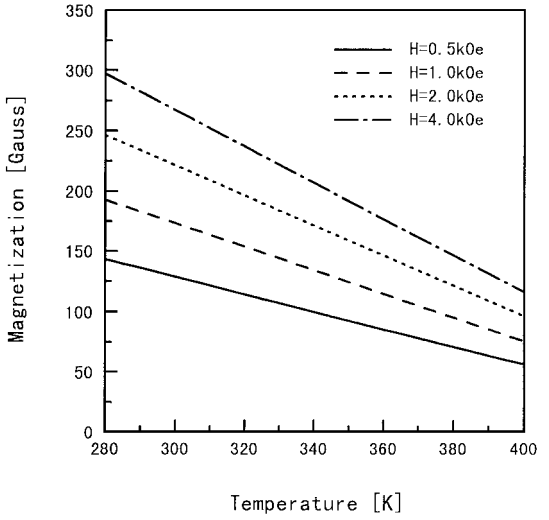

Fig. 1 Temperature-sensitive magnetic fluid (Mn–Zn ferrite in alkyl-naphthalene base).

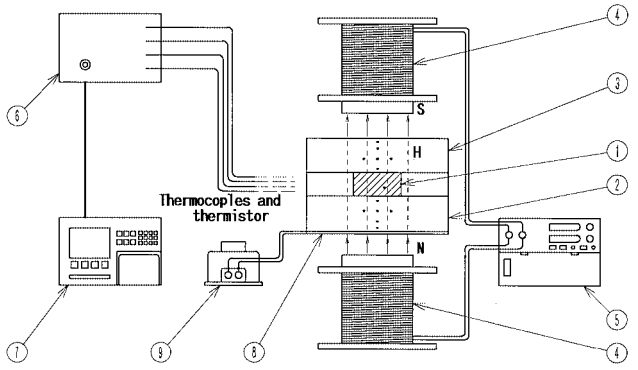

Fig. 2 Experimental apparatus: 1, rectangular box; 2, heating block; 3, cooling block; 4, electromagnet; 5, D.C. current controller; 6, temperature data reader; 7, data processor; 8, ceramic heater; and 9, A.C. controller.

where K is the pyromagnetic coefficient

$$K = \chi/(T_S - T) \tag{2}$$

In Fig. 1, the temperature characteristics for the magnetization of the magnetic fluid are shown, and in Table 1 the basic properties of the magnetic fluid are listed. To characterize the magnetic fluid, the coefficients and constants in Eqs. (1) and (2) are determined from Fig. 1, and they are also listed in Table 1. As shown in Fig. 1, the strong temperature dependence of the magnetization is evident at room temperature.

Figure 2 is a schematic diagram of the experimental apparatus. The magnetic field is imposed vertically on rectangular box 1 (test cell) by electromagnet 4. Box unit 1 is made up with a cavity that contains the magnetic fluid. The bottom of the cavity is heated through copper block 2 by ceramic heater 8 that is attached to the lower

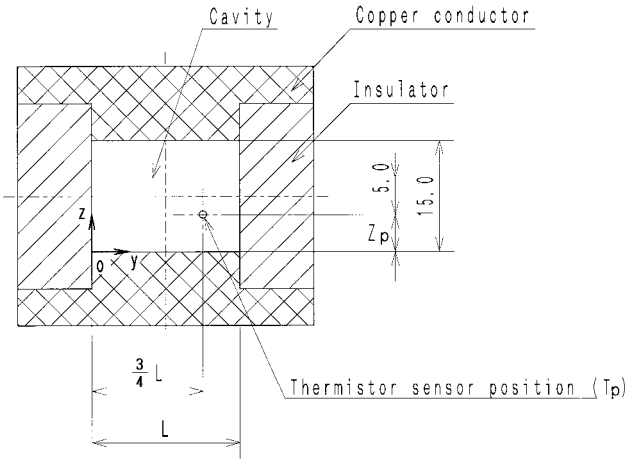

Fig. 3 Rectangular box (cavity), AR = *L*/15.0 (mm): aspect ratio; AR = *L*/15.0 (units in millimeters).

part of the copper block while the upper wall of the cavity is cooled through a copper block whose upper surface is opened to ambient air of constant temperature. Note that the apparatus is placed in a temperature controlled room. The heat transfer rate to and from the cavity is obtained by measuring the temperature gradient in the copper block (by thermocouples distributed as shown in Fig. 2). By knowing the thermal conductivity of the copper and by extrapolating the temperature distribution in the copper blocks, we also obtain the lower wall temperature T_H and the upper wall temperature T_C of the cavity. A representative temperature T_P of the cavity, whose position from the lower wall is z_P, is measured by a thermistor temperature sensor 1.0 mm in diameter. In Fig. 3 the detailed geometry of the rectangular box unit is shown. The unit is made of two copper thermal conductors attached as the upper and lower rigid walls and two insulators that form the rigid side walls. The Cartesian coordinate system (y, z) is chosen so that the origin 0 of the coordinate is at the lower left corner of the cavity (Fig. 3). To characterize the cavity, the aspect ratio AR (ratio between the horizontal length and the vertical length of the cavity) is defined as AR $= L/15.0$, where L are the various horizontal lengths and 15.0 mm is the fixed vertical height of the cavity. Three aspect ratios AR = 1.0, 1.5, and 2.0 are used while keeping the 15.0-mm cavity height constant. Note that the depth of the cavity (width of the rectangular box unit) is taken as 7.5 mm so that the major flow mode of the Benard convection[9] first appears in the (y, z) plane, ensuring the two dimensionality of the cavity.

The unit (Fig. 3) and the heat conduction copper blocks (Fig. 2) are fabricated within ±1% accuracy. The largest measurement error in determining the heat transfer characteristics comes from the temperature measurement, and the margin of error associated with the temperature measurement is approximately ±3.5%, which mainly comes from the temperature measurements in the copper blocks (due to the thermocouple accuracy and the extrapolation of temperature data). The measurement procedure was repeated several times to minimize the error.

III. Numerical Analysis

The system of equations governing the flow of the natural convection of the magnetic fluid are as follows:

$$\nabla \cdot \boldsymbol{v} = 0 \tag{3}$$

$$\rho_0 \frac{\mathrm{D}\boldsymbol{v}}{\mathrm{D}t} = -\nabla p + \eta \nabla^2 \boldsymbol{v} + \mu_0 (\boldsymbol{M} \cdot \nabla)\boldsymbol{H} - \rho \boldsymbol{g} \tag{4}$$

$$\rho_0 C \frac{\mathrm{D}T}{\mathrm{D}t} + \mu_0 T \left(\frac{\partial \boldsymbol{M}}{\partial T} \right)_{V,H} \cdot \frac{\mathrm{D}\boldsymbol{H}}{\mathrm{D}t} = \lambda \nabla^2 T \tag{5}$$

$$\nabla \cdot \boldsymbol{B} = 0, \qquad \boldsymbol{B} = \mu_0 (\boldsymbol{M} + \boldsymbol{H}), \qquad \nabla \times \boldsymbol{H} = 0 \tag{6}$$

where Eq. (3) is the continuity equation for incompressible fluid, Eq. (4) the momentum equation, Eq. (5) the energy equation, and Eq. (6) the Maxwell equations for electrically nonconductive media. The density of the fluid is linearly approximated as follows:

$$\rho = \rho_0[1 + \alpha(T - T_0)] \tag{7}$$

For the numerical calculation, Eqs. (3–6) then are written in nondimensionalized form using the stream function ϕ, the vorticity ζ, and the magnetic field potential ψ as follows:

$$\nabla^2\phi = \zeta \tag{8}$$

$$\frac{\partial\zeta}{\partial t} + (\boldsymbol{v}\cdot\nabla)\zeta = Pr\left\{\nabla^2\zeta - Ra_m[\nabla\times(\boldsymbol{M}\cdot\nabla)\boldsymbol{H}]_y - Ra\frac{\partial T}{\partial z}\right\} \tag{9}$$

$$\frac{\partial T}{\partial t} + (\boldsymbol{v}\cdot\nabla)T - \frac{KT}{H}Ra_m Br\left\{\boldsymbol{H}\cdot\left[\frac{\partial\boldsymbol{H}}{\partial t} + (\boldsymbol{v}\cdot\nabla)\boldsymbol{H}\right]\right\} = \nabla^2 T \tag{10}$$

$$\boldsymbol{H} = \nabla\psi \tag{11}$$

$$(H_0/M_s + \theta)\nabla^2\psi + \nabla\theta\cdot\nabla\psi = 0, \qquad \theta = \chi - K(T - T_0) \tag{12}$$

where the magnetization $\boldsymbol{M}$ is calculated by Eq. (1) from the resultant magnetic and temperature fields. The flow velocity $\boldsymbol{v}$ is obtained according to the stream function ϕ as $\boldsymbol{v} \equiv (v_y, v_z) \equiv [(\partial\phi/\partial z), -(\partial\phi/\partial y)]$, where v_y is the y directional velocity component and v_z is the z directional velocity component. Equation (12) is derived from Maxwell equations (6) and Eqs. (1), (2), and (11) as

$$\nabla\cdot(\boldsymbol{H} + \boldsymbol{M}) = 0$$

for $\boldsymbol{M}^* = \boldsymbol{M}/M_s$ and $\boldsymbol{H}^* = \boldsymbol{H}/H_0$ so that

$$\nabla\cdot(H_0\nabla\psi + M_s\theta\nabla\psi) = 0$$

$$H_0\nabla^2\psi + M_s\nabla\theta\cdot\nabla\psi + M_s\theta\nabla^2\psi = 0$$

The nondimensional parameters in Eqs. (8–10) are[6]

$$Pr = \eta/\rho_0\kappa, \qquad Ra = \rho_0 g\alpha\beta d^4/\kappa\eta$$

$$Ra_m = \mu_0 H M_S d^2/\kappa\eta, \qquad Br = \kappa^2\eta/\lambda\beta d^3 \tag{13}$$

where $\beta = (T_H - T_C)/d$ and d is the height of the cavity ($d =$ 15.0 mm). Note that the Nusselt number obtained from the experiment is the local Nusselt number that can be calculated based on the mean heat flux to the cavity and the local temperature gradient measured by the thermistor sensor at the position of the temperature measuring point in the cell (Fig. 3). Hereafter heat transfer characteristics are presented by the relationship between the local Nusselt number Nu and the Rayleigh number Ra because comparison of results between the experiment and the numerical analysis is only possible for the local Nusselt number. The overall Nusselt number Nu^* can be calculated by the numerical analysis and this will be quoted when necessary. The local Nusselt number Nu and the overall Nusselt number are

$$Nu = -\frac{d}{\Delta T}\left(\frac{T_P - T_H}{z_P}\right), \qquad Nu^* = -\int\frac{1}{\Delta T}\left(\frac{\partial T}{\partial z}\right)_{z=0}\mathrm{d}y \tag{14}$$

where $\Delta T = T_H - T_C$.

The system of equations is then solved using a time-marching explicit finite difference method. In Fig. 4 the basic condition of the numerical calculation is shown. The lower wall of the cavity is heated with temperature of T_H while the upper wall is cooled with temperature T_C. The adiabatic condition is used for side walls. Magnetic boundary conditions $(\boldsymbol{B}_1 - \boldsymbol{B}_2)\cdot\hat{\boldsymbol{n}} = 0$ and $(\boldsymbol{H}_1 - \boldsymbol{H}_2)\times\hat{\boldsymbol{n}} = 0$ are applied[10] at the four rigid walls, where the indices 1 and 2 indicate the outer and inner side of the cavity wall, respectively, and $\hat{\boldsymbol{n}}$ is the unit normal vector at the wall (Fig. 4). The vertical and uniform magnetic field $\boldsymbol{H}_0$, as shown in Fig. 4 (which implies the experimental configuration in Fig. 2), is imposed externally from outside the cavity, where $\boldsymbol{H}_1 = \boldsymbol{H}_0$ and $\boldsymbol{B}_1 = \mu_0\boldsymbol{H}_0$. In the cavity, the internal magnetic field is calculated by solving the magnetic field potential Eqs. (11) and (12) in the iteration sequence using a finite difference method. Equations (8–12) are discretized so that they can be solved by the finite difference method. The size of the mesh used in the numerical simulation is $(40 \times \mathrm{AR} + 1) \times 41$ for i (y directional position index) and j (z direction position index), respectively, and the mesh size $(\Delta y, \Delta z)$ is equally spaced in each direction (Fig. 4). To ensure resolution of the numerical solutions, trial runs were performed using different sized meshes. Representative calculations for Benard convection without the magnetic field showed that the results obtained with a $(40 \times \mathrm{AR} + 1) \times 41$ mesh system made an approximately 1.0% difference to the Nusselt number Nu compared with a 81×81 mesh system. Because the difference due to mesh size was minimal, a $(40 \times \mathrm{AR} + 1) \times 41$ mesh system was used in all calculations. The finite differenc equations for Eqs. (8–12) are formulated with a finite difference of second-order accuracy in space, and the time-marching procedure (explicit Euler method) is used to solve the transient equations. To avoid numerical instability in the nonlinear terms, that is, the convection terms in Eqs. (9) and (10), the upwind Kawamura and Kuwahara scheme[11] of third-order accuracy in space is used as follows for a representative term:

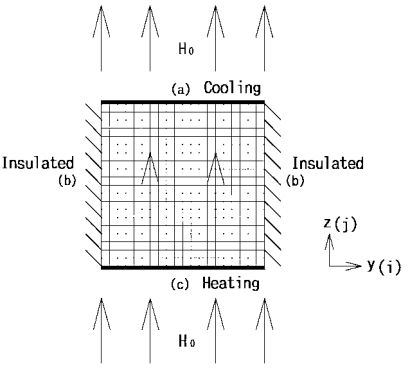

Fig. 4 Mesh configuration for simulation: (a) $T = T_c$, (b) $\partial T/\partial y = 0$, and (c) $T = T_H$.

$$v_{i,j}\frac{\partial\zeta_{i,j}}{\partial y} = v_{i,j}\frac{[-\zeta_{i+2,j} + 8(\zeta_{i+1,j} - \zeta_{i-1,j}) + \zeta_{i-2,j}]}{12\Delta y} + |v_{i,j}|\frac{(\zeta_{i+2,j} - 4\zeta_{i+1,j} + 6\zeta_{i,j} - 4\zeta_{i-1,j} + \zeta_{i-2,j})}{4\Delta y} \tag{15}$$

In each time step, the Poisson equation (8) and the magnetic field potential function (12) are solved using the successive overrelaxation technique with a relaxation factor of 1.8. The convergence of Poisson's equation and the magnetic field potential function are determined with a maximum relative error of less than 1.0×10^{-4}.

IV. Results and Discussions

In Fig. 5, typical transient behavior of the Nusselt number is shown for $\mathrm{AR} = 1.0$ when the Rayleigh number is fixed at $Ra = 5000$ with different magnetic Rayleigh numbers $Ra_m = 0$ (ordinary natural convection), $Ra_m = 3.845 \times 10^5$, and $Ra_m = 9.614 \times 10^5$. The transient calculation is started from the quiescent state of a given temperature difference ΔT with a given magnetic field $\boldsymbol{H}$ so that at the initial stage of the calculation the Nusselt number remains $Nu = 1$, that is, the heat conduction mode of the heat transfer. After some elapsed time (the calculation time) from startup, as shown for example, for $Ra_m = 0$ in Fig. 6, flow instability occurs. Natural convection followed by the convection cell (vortex) appears when the Rayleigh number Ra is larger than a critical value Ra_c (Ref. 9), increasing the heat transfer (Nusselt number Nu) from unity. When the magnetic field is applied, the flow is destabilized soon after the start

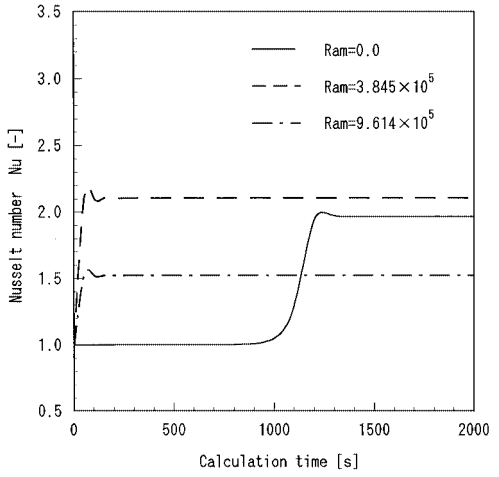

Fig. 5 Transient behavior of *Nu* (AR = 1.0 and *Ra* = 5000).

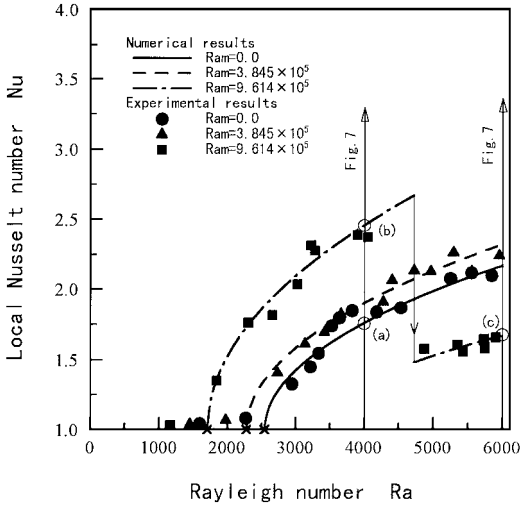

Fig. 6 Heat transfer characteristics (local Nusselt number) for AR = 1.0: experimental and numerical results.

of the calculation, and this trend is more evident when the strength of magnetic field is increased (for larger magnetic Rayleigh numbers Ra_m). However, after the transition from the quiescent state to natural convection, the flow becomes the steady state, reaching an asymptotic value as shown in Fig. 5 for all magnetic Rayleigh numbers Ra_m. Note that hereafter all results presented from the experiment and numerical analysis are at steady state.

In Fig. 6, the heat transfer characteristics for AR = 1.0 are shown as the relationship of Nusselt number vs Rayleigh number, with different magnetic field conditions, where the solid symbols indicate experimental results and the lines are calculated results. As shown in Fig. 6 for both experimental and numerical results, natural convection occurs when the Rayleigh number is increased up to a certain value of the critical Rayleigh number Ra_c, whereas below the critical Rayleigh number, the Nusselt number is unity, showing thermal conduction. The critical Rayleigh number is then estimated by extrapolating the data (both experimental and calculated) by the following relation[12] in the vicinity of the first critical condition:

$$Nu \sim (Ra - Ra_c)^{\frac{1}{2}} \tag{16}$$

As seen in Fig. 6, the calculated results show good agreement with the experimental data and the critical Rayleigh numbers (noted by the × on the horizontal axis in Fig. 6), which are the first transitions of the flow mode and are obtained by fitting both experimental and numerical results with Eq. (16). Note that the calculated results coincide with the critical relation obtained with Eq. (16) very well in the vicinity of the critical condition so that lines appearing in Fig. 6 show both the critical relation and the numerical results to be identical. Note that a comparison of the critical values (without magnetic field, i.e., an ordinary natural convection) with values of published data[13] as listed in Table 2 (where other critical values obtained in the present study are also listed) shows excellent quantitative agreement. The critical Rayleigh number Ra_c decreases when the magnetic field is applied (Fig. 6 and in Table 2), indicating that the magnetic field has a destabilizing hydrodynamic effect on the flow. Also an increase of the magnetic field strength (from $Ra_m = 0$ to 3.845×10^5 and to 9.614×10^5) results in the heat transfer data shifting toward the left, indicating the increase of the heat transfer rate at the supercritical state. The second flow transition occurs for $Ra_m = 9.614 \times 10^5$ at the second critical Rayleigh number, approximately $Ra_{c(2)} = 4725$ (Fig. 6), where a sharp drop of the Nusselt number *Nu* is observed from both the calculated and the analytical results. To verify the experimental results of the heat transfer characteristics as shown in Fig. 6, flow and temperature fields obtained from the numerical analysis are examined next.

Table 2 Critical Rayleigh number at the first flow transition

Ra_m	Value
	AR = 1.0
0	2544.262 (2585.0[a])
3.845×10^5	2277.725
9.614×10^5	1703.795
	AR = 1.5
0	2285.761
3.845×10^5	2078.547
9.614×10^5	1494.612
	AR = 2.0
0	1942.313 (2013.2[a])
3.845×10^5	1682.31
9.614×10^5	1116.307

[a]Comparison with Ref. 13.

In Fig. 7 some representative calculation results of the flow and temperature fields (contours of the stream function and isothermal temperature) associated with the heat transfer characteristics of Fig. 6 (AR = 1.0) are displayed. For clarity, the positions of the variation of Ra_m are indicated in Fig. 6, where the points of the Figs. 7a–7c are indicated by the open circles. As seen in Fig. 7a for $Ra_m = 0$ at $Ra = 4000$, one convection cell, that is, the Benard convection cell, is generated at the supercritical state, and its temperature field becomes distorted toward the flow direction. With the magnetic field $Ra_m = 3.845 \times 10^5$, the shape of the convection cell is almost unchanged while the distortion of the temperature contour lines toward the flow direction become slightly noticeable, showing that the circulation motion of the flow is strengthened by imposing the magnetic field and that the heat transfer is enhanced, as shown in Fig. 6. Further increase of the magnetic field strength $Ra_m = 9.614 \times 10^5$ for $Ra = 4000$ as shown in Fig. 7b results in the convection cell deformation, and further strong circulation motion of the flow appears, increasing the heat transfer further. This phenomenon reflects the experimental data in Fig. 6. Similar trends of the flow and temperature fields persists at $Ra = 6000$, when the strength of the magnetic field is increased from $Ra_m = 0$ to 3.845×10^5. However, when Ra_m is increased to $Ra_m = 9.614 \times 10^5$, as seen in Fig. 7c, two convection cells appear in the flowfield followed by the concave temperature field (which is caused by the downward flow at the center of the cavity), showing that the second flow transition is induced by the presence of a higher magnetic field. Thus, it is verified that the sharp drop of Nusselt number *Nu*, as observed in the experimental data in Fig. 6, is due to this second flow transition. The critical Rayleigh number for the second flow transition is approximately $Ra_{c(2)} = 4725$, as estimated from both the experimental and the analytical results. The sharp drop of Nusselt number *Nu* does not necessary indicate the drop of the overall Nusselt number Nu^*. The separate calculation for overall Nusselt number Nu^* at $Ra_{c(2)} = 4725$ for $Ra_m = 9.614 \times 10^5$ reveals that it is $Nu^* = 2.41$, improving the heat transport capability even when the second flow transition occurred. This is usually the

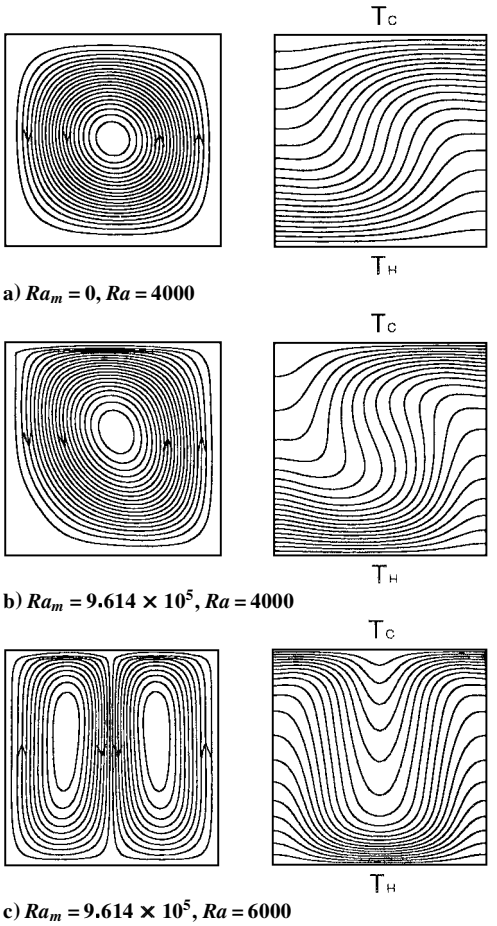

Fig. 7 Flow and temperature fields associated with Fig. 6 (AR = 1.0).

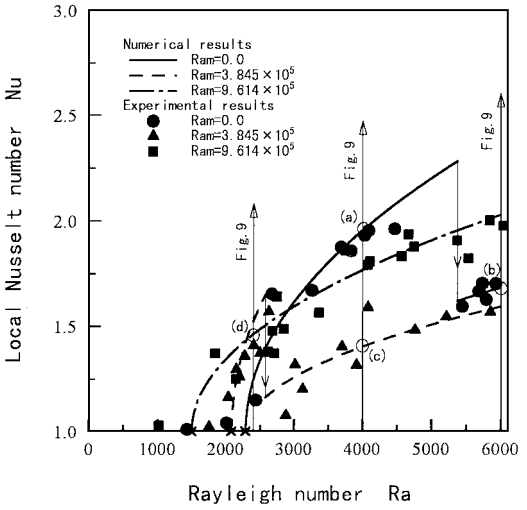

Fig. 8 Heat transfer characteristics (local Nusselt number) for AR = 1.5: experimental and numerical results.

case for improving heat transfer when the higher flow transition is induced[9] due to the higher heat transport by the multiple vortexes in the cavity space. The heat transfer capability associated with the overall Nusselt number Nu^* is discussed later.

In Figs. 8 and 9, the heat transfer characteristics of AR = 1.5 and their associated flowfields at some representative Rayleigh numbers are shown, respectively. It is seen from Fig. 9a, where the flowfield is obtained at $Ra = 4000$ for $Ra_m = 0$, that the basic flow mode after the first flow transition at $Ra_c = 2285$ is one convection cell. However, at approximately $Ra_{c(2)} = 5375$, the second flow transition

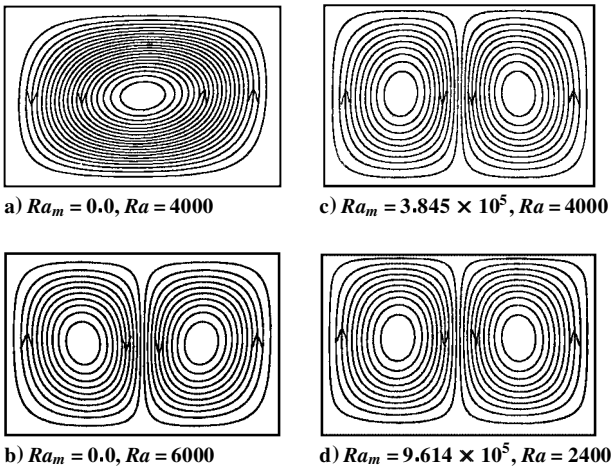

Fig. 9 Flowfields associated with Fig. 8 (AR = 1.5).

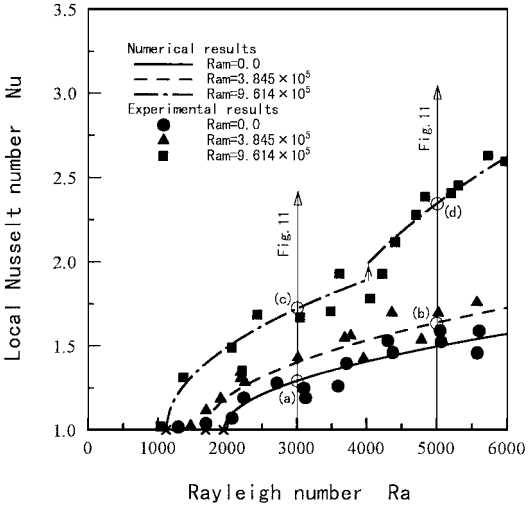

Fig. 10 Heat transfer characteristics (local Nusselt number) for AR = 2.0: experimental and numerical results.

occurs as may be seen from the sharp drop of Nusselt number Nu for $Ra_m = 0$ in Fig. 8. The prevailing flow mode is two convection cells, as shown in Fig. 9b for $Ra = 6000$ after the second critical flow transition for $Ra_m = 0$. By the increase of the magnetic Rayleigh number to $Ra_m = 3.845 \times 10^5$, the first flow transition (the critical Rayleigh number), followed by one convection cell, is shifted to the left side at $Ra_c = 2078$, and at a very early stage at $Ra_{c(2)} = 2575$, the second flow transition occurs, followed by two convection cells as seen in Fig. 9c at $Ra = 4000$. This flow mode persists with further increase of the Rayleigh number within the range of Rayleigh numbers ($Ra = 6000$) studied. However, when the higher magnetic field is applied by $Ra_m = 9.614 \times 10^5$, the first transition mode is that of two convection cells being generated at the critical Rayleigh number $Ra_c = 1494$ (as seen in Fig. 8). The two convection cells' mode (Fig. 9d) at $Ra = 2400$ persists within the range of the Rayleigh number studied. Note that for AR = 1.5 (Fig. 8), the overall heat transfer is indeed improved by imposing the magnetic field due to the higher flow mode, that is, two convection cells, occurring at an early stage of the Rayleigh number, although the sharp drop of the local Nusselt number is seen as stated earlier. To estimate the overall heat transfer characteristics, the overall Nusselt number Nu^* must be calculated from the results of the numerical calculation. For example, for $Ra_m = 3.845 \times 10^5$ at $Ra_{c(2)} = 2575$, the overall Nusselt number Nu^* goes up to 1.30, indicating the higher heat transfer mode when the higher flow transition occurs. This will be discussed later.

In Figs. 10 and 11, results obtained from the experiment and numerical analysis are presented for AR = 2.0 in the way as earlier

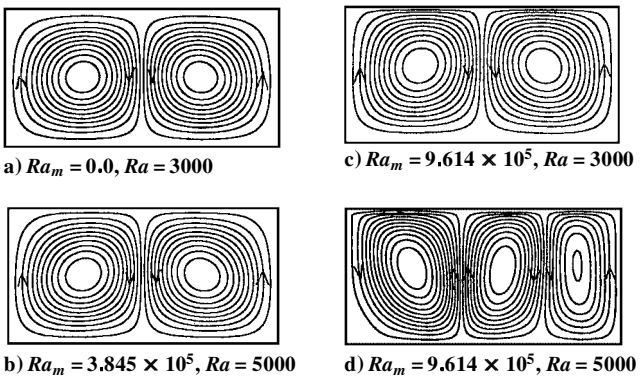

Fig. 11 Flowfields associated with Fig. 10 (AR = 2.0).

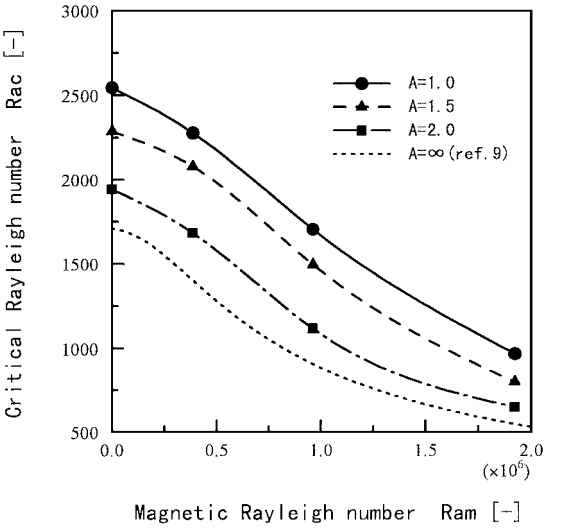

Fig. 12 Relationship between magnetic Rayleigh number and critical Rayleigh number.

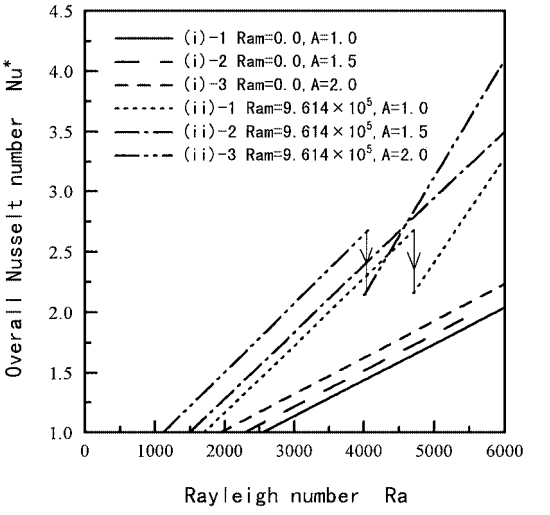

Fig. 13 Heat transfer capability (overall Nusselt number).

results. For $Ra_m = 0$, the basic flow mode of the natural convection is two convection cells (Fig. 11a) at $Ra = 3000$, and this mode persists within the range of the Rayleigh number studied. The first flow transition, followed by the generation of two convection cells, occurs at the critical Rayleigh number $Ra_c = 1942$, which is lower than at AR = 1.0 and 1.5. (The critical Rayleigh number Ra_c for $Ra_m = 0$ at AR = 2.0 agrees with the result of Ref. 13, as seen in Table 2.) An increase from $Ra_m = 0$ to 3.845×10^5 and to 9.614×10^5 (Fig. 10) will only cause the heat transfer characteristic to shift toward the left, keeping the flow mode the same (the continuation of this flow mode can be seen in Fig. 11b at $Ra = 5000$ for $Ra_m = 3.845 \times 10^5$ and Fig. 11c at $Ra = 3000$ for $Ra_m = 9.614 \times 10^5$), whereas the first flow transition occurs at an earlier stage of the Rayleigh number (Table 2). However, when the Rayleigh number is increased to approximately $Ra = 4025$ while keeping $Ra_m = 9.614 \times 10^5$, the sudden jump of Nusselt number Nu is evident in Fig. 10. This is where the second flow transition occurs, that is, $Ra_{c(2)} = 4025$ followed by the generation of three convection cells (Fig. 11d), where the data are taken at $Ra = 5000$ for $Ra_m = 9.614 \times 10^5$. This flow mode can persist for the further increase of Ra Rayleigh number within the range studied. Thus, by examination of the results in Figs. 6, 8, and 10, together with the predicted flow modes obtained by numerical analysis, it is revealed that the flow is destabilized by imposing the magnetic field, and an increase of the magnetic field strength, Ra_m, will cause the transition flow mode to the higher level of flow instability. This means that the imposition of the magnetic field (in the present geometric configuration) has a similar effect of either increasing the Rayleigh number or expanding the aspect ratio of the cavity in ordinary natural convection heat transfer.

In Fig. 12 the critical relation for the first flow transition is shown and the critical relation for the natural convection of the magnetic fluid in the infinite slub,[6] that is, AR = ∞, is used as the reference. As may be seen from Fig. 12, the critical Rayleigh number is a decreasing function of the critical magnetic Rayleigh number for all of the cases, showing that the flow in the two-dimensional cavity can be destabilized by applying the vertical magnetic field. The threshold will be increased by decreasing the aspect ratio, as indicated in Fig. 12, and it is shown that the two-dimensional infinite slab[6] is the most unstable geometric configuration for the imposition of the vertical magnetic field.

Finally, in Fig. 13, the heat transport capability of the magnetic fluid is shown as the relationship between the overall heat transfer, that is, the overall Nusselt number Nu^*, and the Rayleigh number. The scale of the graph is the same as Figs. 5, 7, and 9 (the local Nusselt number Nu) so that comparison is possible. When comparing the local Nusselt numbers in Figs. 6, 8, and 10 and the overall Nusselt numbers in Fig. 13, the heat transfer characteristics are almost the same before the second flow transition occurred. This is because the measuring point of the temperature in the box is fixed in the space to obtain the local heat transfer coefficient. The local flow characteristics at this point are unique once the first flow transition (flow mode appearing from the quiescent conduction mode) is established because the supercritical state is steady state and is always stable. On the other hand, when the second flow transition occurred, the local characteristic of the point in the cavity changes totally due to an alteration of the flow behavior, for example, the flow transition from one convection cell to two convection cells, so that the heat transfer characteristics using the local Nusselt number changes totally, although the basic characteristics of the system (in the sense of the overall heat transfer mode) are presumed. The heat transport capability is largely improved, when the second flow transition followed by a higher flow mode occurred (Fig. 13). This is due to enhancing the heat transfer by the appearance of multiple convection cells[9] and to the energy distribution driving the convection cell. Note that the heat transport capability is largely improved after the second flow transition when the magnetic field is applied, where the changes of curve slopes (in Fig. 13, $Ra_m = 9.614 \times 10^5$, for example) are evident. In the present numerical analysis, the maximum increasing rate of the heat transport capability of the magnetic fluid is approximately 65.0% when the magnetic field is imposed within the range of Rayleigh numbers studied. For example, this enhancement of heat transfer occurred [Fig. 13 for (i)-3 to (ii)-3] at $Ra = 6000$. Finally, note that the total heat transfer rate through the test cell can be estimated by multiplying the aspect ratio AR by the data in Fig. 13, that is, multiplication of the heat transfer area based on the square cavity AR = 1.0.

In the present study, the magnetic field strength applied to the magnetic fluid is limited to a low level in both the experiment and

the numerical analysis because of instrumental limitations and nonconvergence of the numerical solutions. Higher flow modes with unexpected flow patterns, followed by high heat transport capability, would be possible with application of a stronger magnetic field because the phenomena under the consideration are highly nonlinear. Although various magnetic field configurations are interesting to investigate, this is not the scope of the present study, and we shall be reporting on these problems in the future.

V. Conclusions

Experiments were conducted to obtain heat transfer characteristics and their associated flow behaviors of a temperature-sensitive magnetic fluid in two-dimensional rectangular cavities when some magnetic fields were applied. A numerical analysis was adopted to verify the experimental data. From the results of the experiment and the numerical analysis, the following conclusions were drawn:

1) The magnetic field has a destabilizing effect on the flow transition. The critical Rayleigh number is lowered when the magnetic field is applied.

2) Higher flow modes appear when the strength of the magnetic fluid, that is, the magnetic Rayleigh number, is increased, generating multiple flow vortices (natural convection cells).

3) Heat transfer through the two-dimensional cavity is improved when the magnetic field is affected, and this is chiefly caused by either the strong circulation motion of the vortex or the generation of the multiple vortices.

Acknowledgment

This work was partly supported by a grant to the Research Center for Advanced Science and Technology at Doshisha University from the Ministry of Education, Japan. The authors are indebted for the grant.

References

[1]Berkovsky, B. M., *Magnetic Fluids Engineering Applications*, 1st ed., Oxford Univ. Press, New York, 1993, pp. 214–228.

[2]Shiliomis, M. I., "Magnetic Fluids," *Soviet Physics—Advances in Physical Science*, Vol. 17, No. 2, 1974, pp. 153–169.

[3]Stiles, P. J., and Kagan, M., "Thermoconvective Instability of a Ferrofluid in a Strong Magnetic Field," *Journal of Colloid and Interface Science*, Vol. 134, No. 2, 1990, pp. 435–448.

[4]Blennerhassett, P. J., Lin, F., and Stiles, P. J., "Heat Transfer Through Strongly Magnetized Ferrofluids," *Proceedings of the Royal Society of London, Series A: Mathematical and Physical Sciences*, Vol. 433, No. 1887, 1991, pp. 165–177.

[5]Kato, Y., Kawai, H., and Tanahashi, T., "Numerical Flow Analysis in a Cubic Cavity by the GSMAC Finite-Element Method," *Japan Society of Mechanical Engineers International Journal*, Vol. 33, No. 4, 1990, pp. 649–658.

[6]Blums, E., Cebers, A., and Maiorov, M. M., *Magnetic Fluids*, 1st ed., Walter de Gruyter, New York, 1997, pp. 289–341.

[7]Finlayson, B. A., "Convective Instability of Ferromagnetic Fluids," *Journal of Fluid Mechanics*, Vol. 40, Pt. 4, 1970, pp. 753–767.

[8]Yamaguchi, H., Kobori, I., and Uehata, Y., "Natural Convection of Magnetic Fluid in a Rectangular Box," *Journal of Magnetism and Magnetic Materials*," Vol. 201, No. 1–3, 1999, pp. 264–267.

[9]Gershuni, G. Z., and Zhukhovitskii, E. M., *Convective Stability of Incompressible Fluids*, 1st ed., Keterpress Enterprises, Moscow, 1976, pp. 117–142.

[10]Rosensweig, R. E., *Ferrohydrodynamics*, 1st ed., Cambridge Monographs on Mechanics and Applied Mathematics, Cambridge Univ. Press, New York, 1954, pp. 74–98.

[11]Kawamura, T., and Kuwahara, K., "Computation of High Reynolds Number Flow Around a Circular Cylinder with Surface Roughness," AIAA Paper 84-0340, 1984.

[12]Landau, L. D., and Lifshitz, E. M., *Fluid Mechanics*, 1st ed., Vol. 6, Pergamon, New York, 1954, pp. 183–212.

[13]Mizushima, J., "Onset of the Thermal Convection in a Finite Two-Dimensional Box," *Journal of the Physical Society of Japan*, Vol. 64, No. 7, 1995, pp. 2420–2432.